

Research progress on upconversion luminescence and temperature sensing performance based on rare earth-doped $\text{NaYF}_4: \text{Er}^{3+}$

ZHANG YI^{1,2}, ZHOU AIHUA², CAI YUANXUE^{1,2,*}, MING CHENGGUO^{1,2}, PEI YUMIAO²

¹Department of Chemistry, College of Science, Tianjin University of Science & Technology, Tianjin 300457, China

²Research Center for Photonics and Advanced Sensing Technology, College of Science, Tianjin University of Science & Technology, Tianjin 300457, China

Rare earth Er^{3+} mono-doped upconverted sodium crystals were prepared, and the effects of the doping and the reaction time on the structure, morphology and luminescence properties of the materials were investigated, and then these conditions were optimized. The $\text{NaYF}_4: x\% \text{Er}^{3+}$ has a hexagonal crystalline phase with homogeneous morphology. Under 980 nm excitation (with a power of 2.0W) the optimal rare-earth-element doping ratio of $\text{NaYF}_4: 2\% \text{Er}^{3+}$ has a good emission spectrum with color coordinates (0.34, 0.56). The phosphor-dependent luminescence spectra were measured, and the fluorescence intensity ratio (FIR) of its optical thermometer was calculated and fitted [1]. This experimental result lays the foundation for the field of temperature probing of the upconversion luminescence.

(Received August 3, 2024; accepted February 3, 2025)

Keywords: Upconversion luminescence, Temperature sensing, $\text{NaYF}_4: x\% \text{Er}^{3+}$

1. Introduction

Rare-earth luminescent materials in the 1960s have realized the high purity of rare-earth oxides in the television screen, incandescent lamps and other fields of high application, subsequently covered the entire solid luminescent category, and to the anti-counterfeiting [2], biological samples [3] to detect the expansion of the emerging field. Nowadays it has been widely used in many fields, and has become an important research topic in chemical and chemical industry. The upconversion luminescence is a kind of anti-Stokes law of luminescence, called anti-Stokes light. Upconversion luminescent materials are generally doped with single or multiple rare earth ions to improve the upconversion luminescence efficiency. To achieve the best effect of activation, it is crucial to choose a more suitable rare earth ion for the crystal field of material's own crystal field of the rare earth ions, thereby get a high efficiency of fluorescence [4, 5]. Among the temperature-dependent optical properties of rare earth upconversion luminescent materials, temperature sensing based on FIR technology has been widely used by monitoring the emission of two thermally coupled and non-thermally coupled energy levels. The sensing capability of FIR-based optical temperature sensing is affected by two parameters: sensing sensitivity and stability [6].

Rare-earth ion-doped biofluoride materials are the focus and hotspot of upconversion research, due to the low phonon energy and large number of metastable state energy levels of fluoride matrix [7]. The low phonon

energy can reduce the loss of non-radiative leaps, and thus has a higher upconversion efficiency. Therefore the upconversion material based on NaYF_4 is considered to be the best performing luminescent materials. Er^{3+} is also an effective activator ion for upconversion materials [8], which has abundant energy levels that can be excited by infrared photons at 800-1000 nm, and can also be used as a 1.5 μm upconversion material for optical fiber communication [9, 10]. Jie Tang et al. established a novel ketone CTL (Cataluminescence) gas sensor based on $\text{NaYF}_4: \text{Er}^{3+}$ nanocrystals in the experiments of surface-catalyzed luminescence, and the 20% Er^{3+} dopant concentration at a relatively low temperature showed a high CTL intensity indicating that the sensor exhibits good selectivity and fast response [3]; Dan Wang et al. found that indocyanine green dye-sensitized $\text{NaYF}_4: \text{Er}^{3+}$ nanoparticles can improve the excitation efficiency of Er^{3+} , which can be used as a nanoheater materials for thermal imaging and as a stabilizing photoacoustic agent for photoacoustic imaging [11]; Peiyao Wang et al. synthesized core-shell upconversion nanoparticles with high upconversion efficiency using $\text{NaYF}_4: 3\% \text{Er}^{3+}$ to establish a selective and sensitive ratiometric fluorescent nanosensor to detect phototoxicity and carcinogenicity in water [3, 11, 12]. However, now these studies in $\text{NaYF}_4: \text{Er}^{3+}$ fluorescence temperature measurement may not be deep enough, so we need to further study the temperature measurement performance of screen powder.

In this work, a series of $\text{NaYF}_4: \text{Er}^{3+}$ materials were synthesized via a facile hydrothermal method at a relatively low temperature (180 °C) in two hours, four hours and six hours, respectively. We investigated the

effects of different concentrations of Er^{3+} on morphological changes and upconversion luminescence [13]. Therefore, the mono-doped Er-doped NaYF_4 were synthesized, applying to temperature measurement.

2. Experiments and methods

2.1. Raw materials and reagents

Erbium nitrate pentahydrate ($\text{ErNO}_3 \cdot 5\text{H}_2\text{O}$, 99.9%), yttrium nitrate hexahydrate ($\text{YNO}_3 \cdot 6\text{H}_2\text{O}$, 99.5%) products of Shanghai Aladdin Biochemical Science and Technology Co. Ltd.; Ammonium Fluoride (NF_4 , 96.0%) of Shanghai McLean Biochemical Science and Technology Co. Ltd.; Sodium Citrate (99.0%), Sodium Nitrate (NaNO_3 , 99.0%) of Tianjin University, Kewei Company.

Prepare 15 mL of 0.02 mol/L $\text{Er}(\text{NO}_3)_3$ solution and 15 mL of 0.4 mol/L $\text{Y}(\text{NO}_3)_3$ solution.

2.2. Preparation of $\text{NaYF}_4: x\% \text{Er}^{3+}$ by hydrothermal method

In this paper, $\text{NaYF}_4: \text{Er}^{3+}$ will be synthesized by hydrothermal method. Firstly, 2.9410 g of sodium citrate was accurately weighed in a beaker, 10 ml of deionized water was added, and then stoichiometric amounts of $\text{Yb}(\text{NO}_3)_3 \cdot 6\text{H}_2\text{O}$ (0.4 M), $\text{Er}(\text{NO}_3)_3 \cdot 6\text{H}_2\text{O}$ (0.02 M) were added into the above solution and stirred for about 30 min at room temperature, and then 0.0850 g of sodium nitrate and 0.4440 g of ammonium fluoride were added sequentially. The resulting mixture was stirred for another 30 min then transferred into a 50 mL Teflon-lined stainless steel autoclave and heated to 180 °C, and thereafter kept at 180 °C for Y h (Y = 2(Sample 1), 4(Sample 2), 6(Sample 3)), respectively, and the solution was naturally cooled to room temperature after the heating program was completed. The resulting products were collected by centrifugation, washed several times with deionized water and ethanol, and dried at 80 °C for 6 h. After stopping the

program, it was naturally cooled to room temperature, and 3 groups of white powdery solids were obtained and set aside [5].

2.3. Characterization

An ultra-high resolution field emission scanning electron microscope Hitachi SU8600 series (SEM) was used to characterize the micro-morphology and feature size of $\text{NaYF}_4: \text{Er}^{3+}$. A Bruker D8 X-ray diffractometer (Germany) was used to characterize the structure of the samples, and the XRD parameters were set as follows: X-ray source of Cu target, ceramic X-ray tube, voltage ≤ 40 kV, current ≤ 40 mA, step size 0.01, scanning range of $2\theta = 10^\circ - 80^\circ$, scanning speed $5.0^\circ / \text{min}$, scanning range of small angle $0.50 \sim 5.0^\circ$, wide angle $2.0 \sim 150^\circ$ to characterize the phase structure and crystallinity analysis of the prepared $\text{NaYF}_4: \text{Er}^{3+}$. XRD was able to obtain the type of crystal system, crystal structure and crystallinity level of the material. The upconversion emission spectra of the samples were measured on a Horiba fluorog-3 luminescence spectrometer at room temperature using continuous lasers at 980 nm and 1550 nm lasers as excitation sources. In addition, the spectra were measured at different temperatures in the range of 303–483 K using a TAP-02 high temperature fluorescence controller.

3. Results and discussion

3.1. Morphological analysis

The electron micrographs of $\text{NaYF}_4: 2\% \text{Er}^{3+}$ heated for X h (X = 2, 4, 6) are depicted in Fig. 1. It can be seen that the samples have almost the same size distribution, and the particles are uniformly hexagonal prismatic nanoparticles, with a full particle size. However the particles of Sample 3 are not full enough and contain impurities, and the particles of Sample 2 are more full. So the powders of the 4h groups were subjected to XRD.

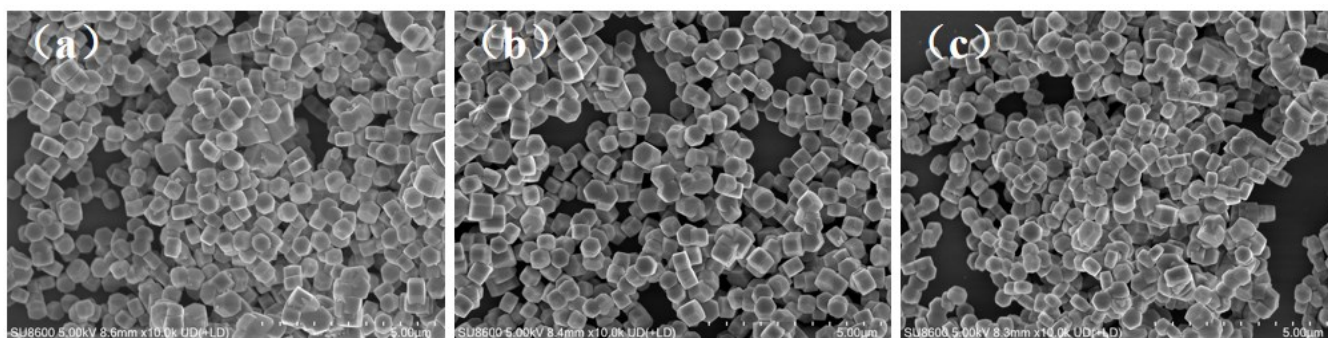


Fig. 1. (a) Sample 1, (b) Sample 2, (c) Sample 3 SEM images of $\text{NaYF}_4: 2\% \text{Er}^{3+}$ heated for 120 min, 240 min, 360 min, respectively

3.2. Crystal structure analysis

Fig. 2 shows the XRD images of $\text{NaYF}_4: x\% \text{Er}^{3+}$ with different Er doping concentrations. It can be seen that with the increase of Er concentration, the phase of the prepared $\text{NaYF}_4: \text{Er}^{3+}$ nanocrystals with the position of the standard

card (JCFDS NO.27-0689) and there are no heterogeneous peaks, which suggests that all the samples are in the pure phase. It is possible that the $\text{NaYF}_4: \text{Er}^{3+}$ nanocrystals were in the pure phase and Er^{3+} successfully replaced Y^{3+} , then doped into the NaYF_4 matrix lattice. The XRD data of the sample show 15 characteristic diffraction peaks in the 2θ

range of 10°-80°, indicating that the NaYF₄: Er³⁺ phosphors synthesized by the hydrothermal method.

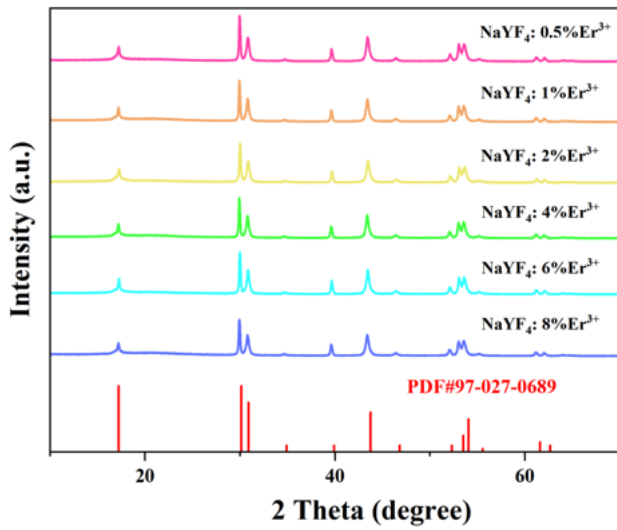


Fig. 2. XRD patterns of NaYF₄: x%Er³⁺ (x = 0.5, 1, 2, 4, 6, 8) heated for 240 min (colour online)

3.3. Optical performance analysis

The emission spectrum of the phosphor at room temperature are displayed in Fig. 3(a). Under the excitation of 980 nm excitation light with a power of 2.0 W, it exhibits the characteristic emission of Er³⁺, with

emission peaks centered about 469 nm, 522 nm, 541 nm and 655 nm corresponding to the transitions of Er³⁺ of ²P_{3/2} → ⁴I_{11/2}, ⁴H_{11/2} → ⁴I_{15/2}, ⁴S_{3/2} → ⁴I_{15/2} and ⁴F_{9/2} → ⁴I_{15/2}, respectively, indicating that Er³⁺ has been successfully doped. With the increase of Er³⁺ concentration, the emission intensity shows an overall trend of increasing and then decreasing, which is guessed to be related to the concentration quenching of Er³⁺ [14]. Fig. 3(b) shows the emission spectra of 2%Er³⁺ co-doped NaYF₄ under different power excitation. The increase of the excitation power did not change the position and morphology of the emission peaks, but enhanced the emission intensity. With the increase of laser power, the luminescence color of the phosphor is mainly concentrated in the yellowish-green light region and does not change significantly. The color coordinates are (0.350, 0.595) when an excitation power is 2W, as shown in Fig. 3(c) [4]. In addition, the number of photons required to jump from the ground state to the excited state under unsaturated conditions can be determined by Eq. (1):

$$I \propto P^n, \quad (1)$$

where I , P , and n represent the emission intensity, power, and number of laser photons [1]. Therefore, the integral intensities of the emission peaks at 528 nm, 539 nm, and 653 nm are calculated. And the logarithmic relationship between the power and the integral intensity is given in Fig. 3(d). The n values obtained from the fitting calculations are 1.94, 1.99 and 1.38.

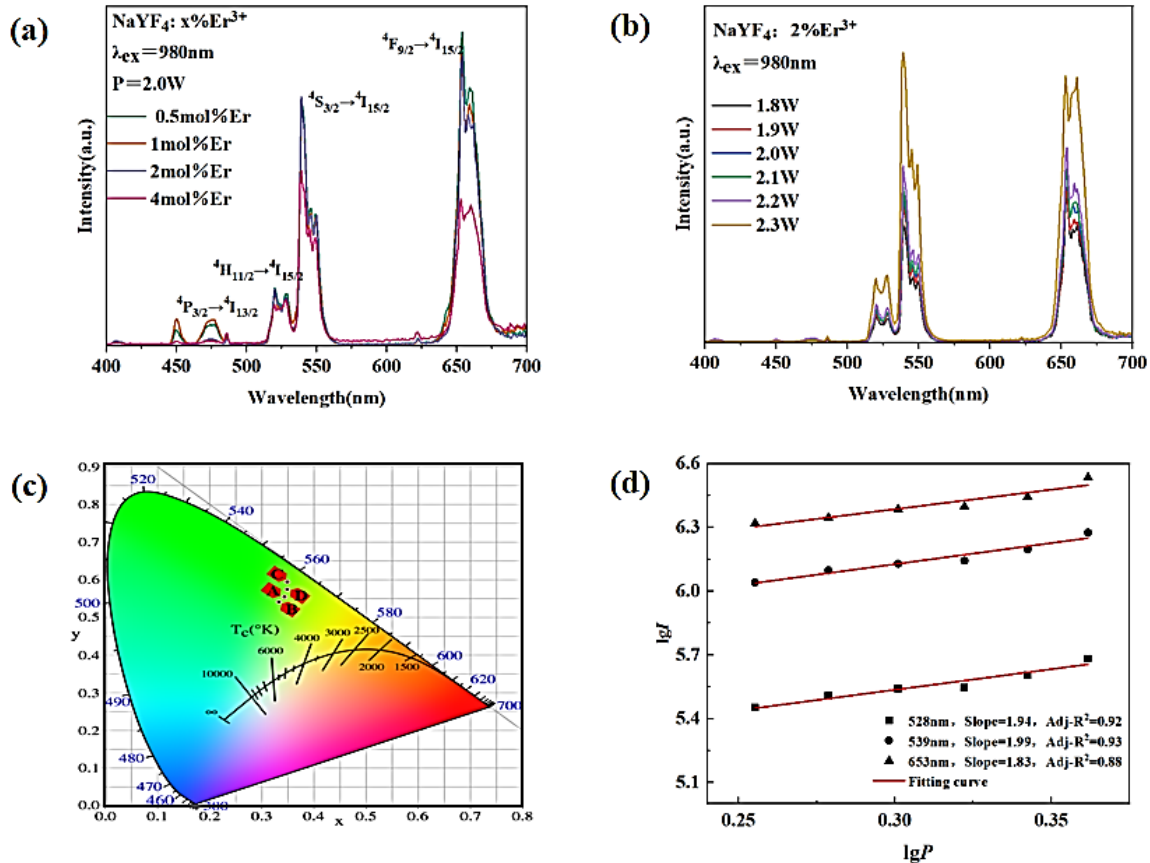


Fig. 3. (a) Fluorescence spectra of NaYF₄:x%Er³⁺ phosphor under the excitation of 980 nm laser; fluorescence spectra (b) and chromaticity diagrams (c) of NaYF₄:2 mol%Er³⁺ phosphor at different powers; (d) relationship between lgI and lgP (colour online)

Under the excitation of 1550 nm excitation light with a power of 3.0 W, the phosphor exhibits the characteristic emission of Er^{3+} , with sharp emission peaks centered at about 541 nm and 655 nm corresponding to the jumps of ${}^4\text{S}_{3/2} \rightarrow {}^4\text{I}_{15/2}$ and ${}^4\text{F}_{9/2} \rightarrow {}^4\text{I}_{15/2}$ of Er^{3+} , respectively, and there are also emission peaks with small amplitude centered at about 522 nm corresponding to the jumps of ${}^4\text{H}_{11/2} \rightarrow {}^4\text{I}_{15/2}$ of Er^{3+} , respectively. With the increase of Er^{3+} content, the emission intensity shows an overall trend of increasing and then decreasing. Fig. 4(b) shows the emission spectra of 2% Er^{3+} co-doped NaYF_4 under different power excitation, and the increase of excitation power did not change the position and morphology of the emission peaks, but enhanced the emission intensity of each leap. With the increase of laser power, the luminous color of the phosphor is mainly concentrated in the yellowish-green light region and does not change

significantly, and the color coordinates are (0.3815, 0.6025) at an excitation power of 3.0 W, as shown in Fig. 4(c). Similarly, the logarithmic relationship between power and integral intensity under the excitation of 1550 nm laser is shown in Fig. 4(d). In addition, it can also be found that when the concentration of Er^{3+} gradually increases, the colour coordinates will continue to move towards the yellow light region, in which 1% Er^{3+} has a stronger tendency to favour yellow light, and it is guessed that it has a good application prospect in the field of anti-counterfeiting. As shown in Fig. 5, (a) for the natural light to take NaYF_4 : 1% Er^{3+} sample 0.1 g, add 0.1 ml of deionised water, shaking well and then speak the mixed solution coated on clean A4 paper, drying in a dim environment using a 980 nm laser irradiation of the coated samples presented as shown in Fig. 5 (b) strong fluorescent green.

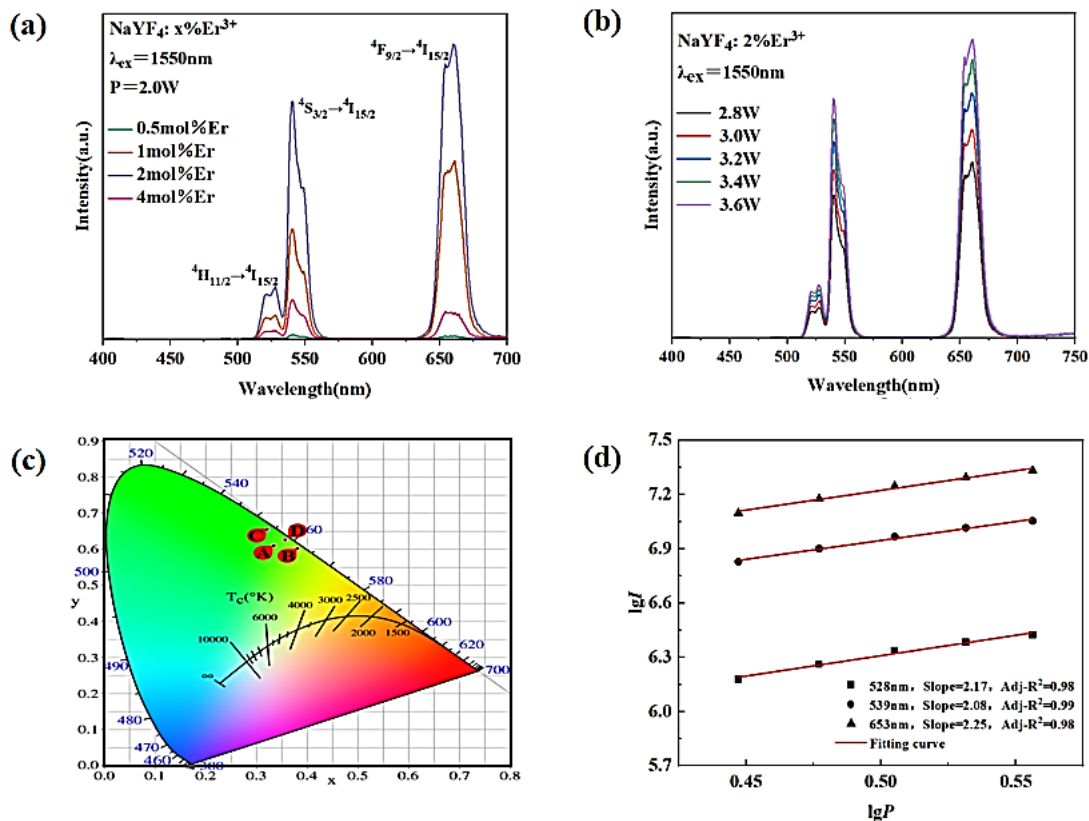


Fig. 4. (a) Fluorescence spectra of $\text{NaYF}_4: x\% \text{Er}^{3+}$ phosphor under the excitation of a 1550 nm laser; fluorescence spectra (b) and chromaticity diagrams (c) of $\text{NaYF}_4: 2 \text{ mol}\% \text{Er}^{3+}$ phosphor at different powers; (d) relationship between $\lg I$ and $\lg P$ (colour online)

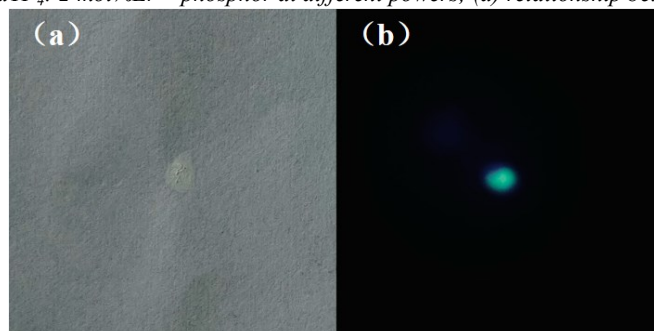


Fig. 5. (a) The $\text{NaYF}_4: 1\% \text{Er}^{3+}$ sample powder prepared as a solution on A4 paper after blotting and drying, (b) a strong fluorescent green colour under 980 nm laser irradiation in a dimly lit environment (colour online)

The energy level leap schematic shown in Fig. 6. It can classify the up-conversion fluorescence spectra in figure into three main fluorescence bands: (1) The up-conversion at 519 nm-529 nm corresponds to ${}^4I_{11/2} \rightarrow {}^4I_{15/2}$ energy level jump, with center wavelengths of 520 nm and 528 nm; (2) the upconversion at 535 nm-558 nm corresponds to the ${}^4S_{3/2} \rightarrow {}^4I_{15/2}$ energy level jump, with center wavelengths of 539 nm and 540 nm; (3) the upconversion at 640 nm-680 nm corresponds to the ${}^4F_{9/2} \rightarrow {}^4I_{15/2}$ energy level jump, with center wavelengths of 654 nm and 661 nm. Fluorescence emission peaks and center wavelengths are also observed to remain largely unchanged, but due to the influence of the dopant ions by the matrix crystal field and lattice vibration, there is a special 465 nm-484 nm upconversion under the 980 nm excitation light corresponding to the ${}^2P_{3/2} \rightarrow {}^4I_{11/2}$ energy level jump with a center wavelength of 477 nm [15].

Under 980 nm excitation light, it can excite the electrons of Er³⁺ ions from ${}^4I_{15/2}$ energy level to ${}^4I_{11/2}$ energy level, or from ${}^4I_{11/2}$ energy level to ${}^4F_{7/2}$ energy level, which can occur the two-photon process of the Er³⁺ ions. Under the excitation light of 1550 nm, the electrons of Er³⁺ ions can excite the electrons from ${}^4I_{15/2}$ energy level to the ${}^4I_{11/2}$ energy level, or from the ${}^4I_{11/2}$ energy level to the ${}^4F_{7/2}$ energy level, and then from ${}^4F_{7/2}$ energy level to ${}^2D_{3/2}$, and thus the three-photon process of the Er³⁺ ions can occur. When the Er³⁺ ion in the crystalline material leaps to the higher energy level ${}^4F_{7/2}$, by subsequent spontaneous radiation from ${}^4F_{7/2}$ or radiation-free relaxation from ${}^4F_{7/2}$ leaps to other lower energy levels and then luminescent radiation, higher photon energy, shorter wavelength fluorescence can be generated, thus realizing up-conversion luminescence.

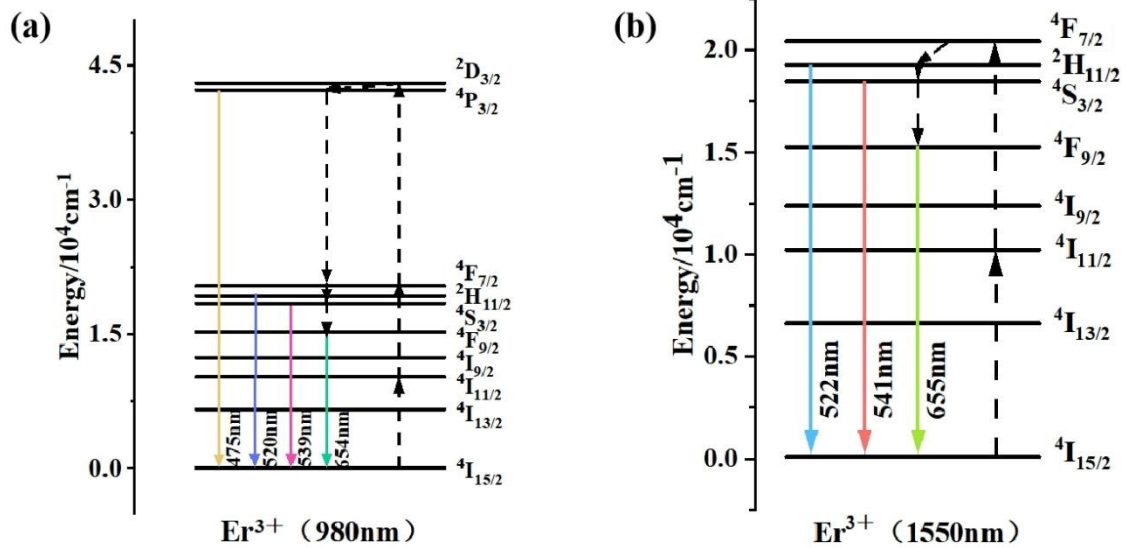


Fig. 6. Energy level structure and upconversion luminescence mechanism of Er³⁺ ion under (a) 980 nm and (b) 1550 nm excitation light excitation (colour online)

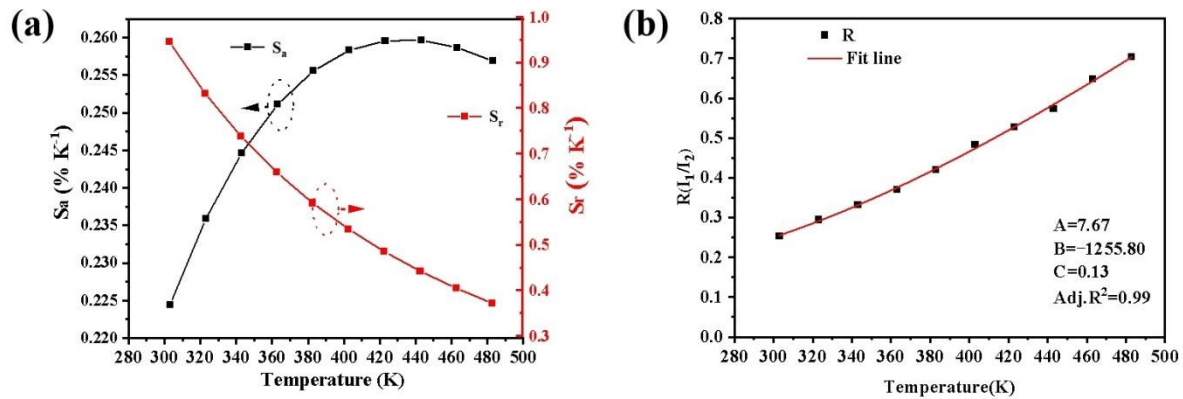


Fig. 7. FIR (a) and sensitivity (b) of NaYF₄: 2%Er³⁺ phosphor (colour online)

In addition, the energy levels (${}^4S_{3/2} \rightarrow {}^4I_{15/2}$ and ${}^4F_{9/2} \rightarrow {}^4I_{15/2}$) of Er³⁺ as a pair of thermally coupled energy levels can be used to design non-contact optical thermometers based on the FIR technique due to their different corresponding to temperature [16].

The FIR (R_{FI}) values at different temperatures are calculated as follows Eq. (2):

$$R_{FI} = \frac{I_{520}}{I_{540}} = B e^{(-\Delta E/kT)} + C \quad (2)$$

where I_1 and I_2 represent the fluorescence intensity integrals of 513-533 nm (${}^2H_{11/2} \rightarrow {}^4I_{15/2}$) and 533-560 nm (${}^4S_{3/2} \rightarrow {}^4I_{15/2}$), respectively. C is the constant of proportionality, ΔE is the energy gap between 520 nm and 540 nm; and k_B and T denote the Boltzmann's constant and the absolute temperature [17]. The fitting of the data points according to Eq. (1) is shown in Fig. 8. From the figure, it can be seen that the pair of energy levels ${}^2H_{11/2}$ and ${}^4S_{3/2}$ is consistent with the characteristics of thermally coupled energy levels, and the good fit of the data points to the curves further demonstrates the reliability of the experimental data. The $\text{NaYF}_4: 1\% \text{Er}^{3+}$ crystals were fitted with the equation $R = 7.67 \exp(-1255.80/T) + 0.13$, with a fit degree as high as 0.999, which corresponds to the parameter representation of $B = 7.67$, $-\Delta E/k = 1255.80$, $C = 0.13$, and the value of ΔE was calculated to be 1733.75 cm^{-1} (as shown in Fig. 7(a)). For this phosphor, the magnitude of change in FIR is small with the increase in temperature, which means that the rate of change in the emission intensity of this phosphor will be relatively close. In addition, the absolute sensitivity (S_a) and relative sensitivity (S_r) of the optical thermometer can be estimated by the Eq. (3) and Eq. (4):

$$S_r = \frac{1}{R} \left(\frac{dR}{dT} \right) = 100\% \times \frac{\Delta E}{kT^2} \times \frac{Be^{(-\Delta E/kT)}}{Be^{(-\Delta E/kT)} + C} \quad (3)$$

$$S_a = \frac{dR}{dT} = \frac{\Delta E}{kT^2} \times (Be^{(-\Delta E/kT)}) \quad (4)$$

Among them, the formula for absolute sensitivity is interpreted as the rate of change of fluorescence intensity ratio to temperature, and relative sensitivity is interpreted as the rate of change of fluorescence intensity ratio to temperature divided by fluorescence intensity ratio [13]. The sensitivity curve of $\text{NaYF}_4: 2\% \text{Er}^{3+}$ phosphor was fitted according to the above two equations, as shown in Fig. 7. It can be calculated from the data that S_a increases gradually with increasing temperature and reaches a maximum value of $0.26\% \text{ K}^{-1}$ (423-433 K), while S_r decreases gradually with increasing temperature and reaches a maximum value of $0.95\% \text{ K}^{-1}$ (303 K), as shown in Fig. 7(b). Since the absolute sensitivity is greatly affected by the material concentration, excitation and detection system, it is difficult to accurately measure the temperature measurement performance of the absolute sensitivity, and the relative sensitivity is the current means of evaluating the merits of the temperature sensing performance. Taking into account the comprehensive considerations, the $\text{NaYF}_4: 2\% \text{Er}^{3+}$ phosphor meets the requirement of high sensitivity within the temperature range of 303-483 K. Table 1 demonstrates the fluorescence temperature sensing performance of Er-doped substrates. Taking into account the comprehensive considerations, the $\text{NaYF}_4: 2\% \text{Er}^{3+}$ phosphor meets the requirement of high sensitivity compared to other matrices.

Table 1. Comparison of temperature sensing performance of single-doped Er^{3+} phosphor or co-doped phosphor with Er^{3+} and Yb^{3+}

Samples	Temperature range/K	Jump (e.g. quantum leap in spectroscopy)	$S_{r \max} / (\% \text{K}^{-1})$	Ref.
$\text{NaGdF}_4: \text{Er}^{3+}, \text{Yb}^{3+}$	303-573	${}^2H_{11/2} \rightarrow {}^4I_{15/2}, {}^4S_{3/2} \rightarrow {}^4I_{15/2}$	0.0021	[18]
$\text{YNbO}_4: \text{Er}^{3+}, \text{Yb}^{3+}$	298-673	${}^4H_{11/2} \rightarrow {}^4I_{15/2}, {}^4S_{3/2} \rightarrow {}^4I_{15/2}$	0.0072	[19]
$\text{Y}_2\text{O}_3: \text{Er}^{3+}, \text{Yb}^{3+}$	293-723	${}^4F_{13/2} (\text{Yi}) \rightarrow {}^4I_{15/2} (\text{Zi}), {}^4F_{13/2} (\text{Y}_1) \rightarrow {}^4I_{15/2} (\text{Z})_1$	0.03	[20]
$\text{BaMoO}_4: \text{Er}^{3+}, \text{Yb}^{3+}$	293-553	${}^4F_{13/2} (\text{Yi}) \rightarrow {}^4I_{15/2} (\text{Zi}), {}^4F_{13/2} (\text{Y}_1) \rightarrow {}^4I_{15/2} (\text{Z})_1$	0.065	[21]
$\text{Ba}_5\text{Gd}_8\text{Zn}_4\text{O}_{21}: \text{Er}^{3+}, \text{Yb}^{3+}$	298-490	${}^4F_{9/2(1)} \rightarrow {}^4I_{15/2}, {}^4F_{9/2(2)} \rightarrow {}^4I_{15/2}$	0.16	[22]
$\text{BaY}_2\text{O}_4: \text{Er}^{3+}, \text{Yb}^{3+}$	298-573	${}^4F_{9/2(1)} \rightarrow {}^4I_{15/2}, {}^4F_{9/2(2)} \rightarrow {}^4I_{15/2}$	0.19	[23]
$\text{NaYF}_4: \text{Er}^{3+}$	303-483	${}^4S_{3/2} \rightarrow {}^4I_{15/2}, {}^4F_{9/2} \rightarrow {}^4I_{15/2}$	0.26	This work

4. Conclusion

In this paper, we synthesized $\text{NaYF}_4: \text{Er}^{3+}$ nanocrystalline materials using a hydrothermal method. The strongest upconversion luminescence intensity was determined by spectral analysis at a concentration of 2% of Er^{3+} ions. The $\text{NaYF}_4: \text{Er}^{3+}$ nanocrystalline material proved to exhibit good luminescence performance, and the ΔE was calculated to be 1733.75 cm^{-1} . In addition, the maximum S_a and S_r values were $0.26\% \text{ K}^{-1}$ and $0.95\% \text{ K}^{-1}$ (303 K), and the absolute sensitivity increased with the increase of temperature. The above results show that

$\text{NaYF}_4: \text{Er}^{3+}$ phosphors can be useful in the field of temperature detection. These unique multi-modal, multi-color spectral properties make the sample as a promising luminescent materials for advanced anti-counterfeiting, graphic marking and information encryption applications.

Acknowledgements

This work was supported by the National Natural Science Foundation of China (No. 61405146, 12174206,

12104340); the National Key R&D Plan (No. 2021YFB3502701); the Tianjin Research Program of Application Foundation and Advanced Technology (No. 14CQNJC01700); the Sino-Singapore Tianjin Eco-city 2019 Support Technology Company Upgrade Project (No. CSTJECO2019TSMES6).

References

- [1] H. Gao, Q. Chen, W. Chen, X. Min, B. Ma, *Chinese Journal of Luminescence* **44**(11), 1958 (2023).
- [2] B. Zhou, K. Fan, J. Zhai, C. Jin, L. Kong, *Adv. Sci. (Weinh)* **10**(30), 2303527 (2023).
- [3] D. Wang, D. Wang, A. Kuzmin, A. Pliss, W. Shao, J. Xia, J. Qu, P. N. Prasad, *Advanced Optical Materials* **6**(12), 1701142 (2018).
- [4] A.-H. Li, G. Chen, *Journal of Physics D: Applied Physics* **53**(4), 043001 (2020).
- [5] P. S. May, M. Berry, *Methods Appl. Fluoresc.* **7**(2), 023001 (2019).
- [6] L. Xuecheng, H. Haoyue, L. Liang, *Physica Scripta* **99**(5), 055510 (2024).
- [7] L. Su, F. Ma, Z. Chen, Q. Lü, Z. Li, H. Yin, Z. Zhang, H. Zhou, Q. Gao, Y. Xu, Y. U. P. M. Tam, *Journal of Inorganic Materials* **39**(3), 330 (2024).
- [8] B. Vasudevan, A. J. O. Sivasubramanian, *Optoelectron. Adv. Mat.* **9**(5-6), 608 (2015).
- [9] M. Lipson, T. Chen, D. Lim, A. Luan, A. Agarwal, J. Michel, K. Wada, L. J. Kimerlin, *Journal of Luminescence* **87**, 323 (2000).
- [10] Y. Cai, C. Ming, M. Pei, Xiaobin Ren, Zhengyang Yu, Yueting Qin, Liquan An, *Optoelectron. Adv. Mat.* **11**(9-10), 565 (2017).
- [11] Y. Gao, S. Zhan, Y. Liu, *Optics Communications* **285**(13-14), 3150 (2012).
- [12] J. Tang, H. Song, B. Zeng, L. Zhang, Y. Lv, *Sensors and Actuators B: Chemical* **222**, 300 (2016).
- [13] A. Zhou, F. Song, W. Yao, Y. Han, F. Song, W. Wu, C. Ming, D. Ju, A. Khan, *Journal of Alloys and Compounds* **775**, 457 (2019).
- [14] A. Zhou, F. Song, Y. Han, F. Song, D. Ju, X. Wang, *CrystEngComm* **20**(14), 2029 (2018).
- [15] S. Singh, S. Kachhap, A. K. Singh, S. Pattnaik, S. K. Singh, *Methods Appl. Fluoresc.* **10**(4), 044004 (2022).
- [16] C. Dubey, A. Yadav, D. Baloni, S. Kachhap, S. K. Singh, A. K. Singh, *RSC Adv.* **13**(30), 20975 (2023).
- [17] A. K. Singh, P. K. Shahi, S. B. Rai, B. Ullrich, *RSC Advances* **5**(21), 16067 (2015).
- [18] J. Zhu, P. Du, J. S. Yu, *Applied Physics A* **126**(3), 1 (2020).
- [19] Y. Tian, Y. Tian, P. Huang, L. Wang, Q. Shi, C. E. Cui, *Chemical Engineering Journal* **297**, 26 (2016).
- [20] N. Rakov, G. S. Maciel, *Journal of Luminescence* **199**, 293 (2018).
- [21] R. Lei, X. Liu, F. Huang, D. Deng, S. Zhao, H. Xu, S. Xu, *Optical Materials* **86**, 278 (2018).
- [22] H. Suo, C. Guo, T. Li, *The Journal of Physical Chemistry C* **120**(5), 2914 (2016).
- [23] G. Xiang, X. Liu, Q. Xia, S. Jiang, X. Zhou, L. Li, Y. Jin, L. Ma, X. Wang, J. Zhang, *Inorg. Chem.* **59**(15), 11054 (2020).

*Corresponding author: yuanuxe_cai@tust.edu.cn